J2.3 NUMERICAL STUDY OF EFFECTS OF ATMOSPHERE TEMPERATURE PROFILE ON WILDFIRE BEHAVIOR

Chunmei Xia[1]*, M. Yousuff Hussaini[1], Philip Cunningham[1], Rodman R. Linn[2], and Scott L. Goodrick[3]
[1]The Florida State University, Tallahassee, Florida
[2] Los Alamos National Laboratory, Los Alamos, New Mexico
[3] USDA Forest Service, Southern Research Station, Athens, Georgia

1. INTRODUCTION

The vertical temperature profile and hence the stability in the atmosphere near the ground varies significantly between day and night. Typically, the potential temperature at the surface is higher than that above the ground during the day and lower than that above the ground during the night. Such differences in the vertical temperature profile might act to accelerate or slow down wildfire propagation accordingly. It is believed that low-level atmospheric stability influences wildfire behavior. Both observational studies (e.g., Werth & Ochoa 1993; Potter 1996) and numerical studies (e.g., Jenkins 2001) have been performed to compare with and verify the Haines Index (Haines 1988), which is a severity index for wildland fires based upon the stability and moisture content of the lower atmosphere. However, few of these studies isolated the effects of low-level atmospheric stability on fire behavior (e.g., spread rate, intensity, plume structure and evolution).

In the present study, a coupled atmosphere-fire model, HIGRAD/FIRETEC, developed at the Los Alamos National Laboratory (Linn 1997; Reisner et al. 2000; Linn et al. 2002), is employed to examine the effects of the atmospheric potential temperature profiles on the rate of spread (ROS) of fire, in addition to the potential temperature and velocity fields in the domain. For this purpose, we studied five different types of vertical potential temperature profile. One of them represents the neutral stability case; two of them represent stable cases with potential temperature increasing with height; the other two represent the unstable cases with potential temperature decreasing with height. Linear and piecewise linear temperature profiles are assumed for an ambient wind speed equal to 2.22 m s^{-1} (corresponding to 5 mph).

2. NUMERICAL MODEL

Details of the HIGRAD/FIRETEC model are given in Linn (1997), Reisner et al. (2000), and Linn et al (2002) and are not repeated here. The domain used in the simulations to be shown here is a rectangular box that is 360 m in the horizontal wind direction (*x*), 240 m in the horizontal crosswind direction (*y*), and 615 m in the vertical direction (*z*). The size of one grid cell is 2 m x 2 m horizontally, and there are 41 stretched grids vertically with a smaller cell size near ground. The vertical grid size is about 1.5 m near the ground. At $x = 0$ a uniform incoming velocity is specified; at $x = 360$ m, $y = 0$ m, and $y = 240$ m, outflow boundary conditions are specified; at $z = 615$ m there is an outflow boundary with a damping layer; and at $z = 0$ m there is a wall with vegetation drag.

The fuel is distributed uniformly on the bottom of the domain. The ignition area is specified as a narrow region (2 x 20 cells) within 78 m < x < 82 m and 100 m < y < 140 m. The fuel properties are identical to those described in Linn et al. (2002) as being representative of tall grass. The incoming wind speed is taken to be 2.22 m s^{-1} (i.e., 5 mph).

To determine the rate of spread (ROS), we first locate the fire front based on the ground temperature contour at each time instant. In the interface area of burning and unburned zones, the fire front is where the temperature reaches the fire front temperature T_{ffront}. ROS is calculated from the first derivative of the edge of fire front with respect of time, *t*, recorded from *t*1 to *t*2. Here we use T_{ffront} = 500 K. For the overall ROS, *t*2 is the current time and *t*1 = 0.

3. SIMULATIONS

In order to study the interactions between atmospheric stability and fire behavior, we performed simulations for five vertical profiles of potential temperature, as shown in Fig. 1. The first simulation is the neutral stability case, where the ground potential temperature is the same as that at the upper boundary. The second simulation is referred to as stable case I, in which the atmosphere has a linear potential temperature profile with the ground potential temperature 10 K lower than that at the top boundary. The third simulation is referred to as stable case II, in which

* Corresponding author address:
Chunmei Xia, 400 Dirac Science Library, CSIT,
Florida State University, Tallahassee, FL 32306
Email: xia@csit.fsu.edu

the atmosphere has a piecewise linear potential temperature profile. The potential temperature increases linearly by 7 K from z = 0 to z = 100 m, and by a further 3 K from z = 100 m to z = 615 m. The fourth simulation is referred to as unstable case I, in which atmosphere has a linear potential temperature profile with the ground potential temperature 10 K higher than that at the top boundary. The fifth simulation is referred to as unstable case II; similar to stable case II, the potential temperature decreases linearly by 7 K from z = 0 to z = 100 m, and by a further 3 K from z = 100 m to z = 615 m. For each of the five cases, we run the simulation to 240 s.

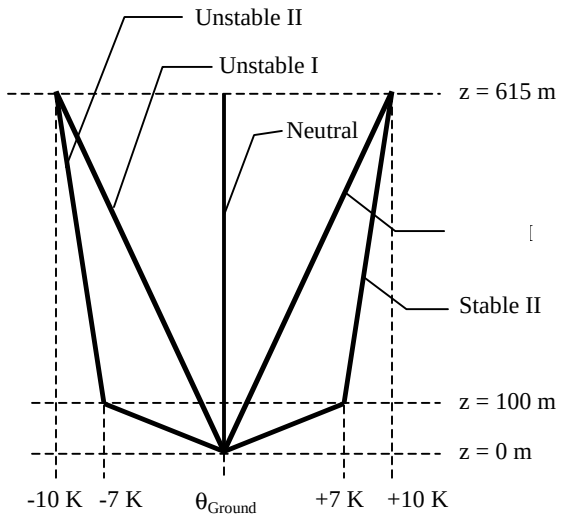

Figure 1. Vertical potential temperature profiles used in the simulations

4. RESULTS

The potential temperature and streamlines in the domain and the bulk ground fuel density at t = 120 s and t = 240 s are shown in Fig. 2 for the neutral stability case. Figure 3 shows the results for the stable case I, and Fig. 4 shows the results for the stable case II. The results for the unstable case I and unstable case II are shown in Fig. 5 and Fig. 6, respectively. The color map for the potential temperature is blue–red–yellow from low temperature to high temperature. For the bulk fuel density, the green color corresponds to the initial fuel density; the darker the color, the less fuel is remaining at that location.

For the neutral stability case, the fire spreads primarily in the wind direction and the shape of the fire front changes from the original straight line to a parabolic shape at a later time. For the two stable cases, the shape of the fire front becomes more conical than the neutral case at later times. Also, the plumes in the stable cases do not penetrate as high above the ground as do those in the neutral case; this is particularly true of stable case II. In the unstable cases, it is apparent that the fire propagates not only in the downwind direction, but also in the lateral direction. In these cases, the fires exhibit more of a self-influenced behavior because the buoyancy effects are more important. In addition, the length of the fire front is greater in the unstable cases than in the stable and neutral cases. Comparing the images at t = 120 s, we can see that the shape of the fire front becomes parabolic even at this early stage for the unstable cases.

The average overall rate of spread (ROS) in the downwind direction over the 20 cells for all five cases are shown in Fig. 7. For the sake of completeness, in Fig. 9 we also show the variation of the maxima in potential temperature in the domain with time for all the cases.

In all of the simulations, as the fire develops more heat is released to the air, and the buoyancy-driven convection starts to take effect. This convection enhances the heat transport and fuel combustion in the burning area. It is evident that the ROS and maximum potential temperature for the stable cases are remarkably similar to those of the neutral case. Indeed, at this low wind speed, the effects of stability are not at all obvious in the comparison between the stable and neutral cases. In contrast, the effects of an unstable profile are more apparent for this low wind speed, as seen in Fig. 7 for the two unstable cases. After the developing period, the buoyancy-driven effects play a more important role for the unstable case II. Initially, the presence of instability allows larger buoyancy-induced vertical velocities and thus more turbulence and higher intensity fire lines. However, at later times the stronger vertical velocities act to block the mean flow and cause the fire line width to shrink and the total heat production to drop. Therefore, the rate of spread in the wind direction and the maximum temperature are lower for the unstable case II than the unstable case I at later times, whereas both of them are higher than those for the neutral case. In addition, the presence of instability appears to allow the fire to propagate in all directions more easily.

5. DISCUSSION AND CLOSING REMARKS

Fire spread is coupled with and determined by motion in the atmosphere. Wind-driven and buoyancy-driven flows interact and compete with each other to determine the fire behavior. If the

buoyancy-driven flow becomes the dominant convection mechanism in the domain, the fire appears to spread in all directions; if the wind-driven flow becomes the dominant mechanism, the fire tends to propagate mainly in the wind direction.

In the neutral and stable cases, the fire propagates primarily in the wind direction. The stable case inhibits the buoyancy effects and makes the fire more predictable because it mainly propagates in the wind direction. Nevertheless, the presence of stability does not appear to affect fire spread significantly in comparison with the neutral case, although the structure of the associated plumes is somewhat different. In the unstable cases, the rate of spread is higher compared with the neutral and stable cases, and the fire propagates not only in the wind direction, but also in the lateral direction.

In this paper, we have attempted to isolate the effects on fire behavior of atmospheric stability by using the same ground temperature for all of the profiles. In reality, the diurnal variation in low-level stability is driven by diurnal variations in the ground temperature. In this regard, observed differences in fire behavior under stable, neutral, or unstable environmental conditions are likely to be attributed to a combination of effects associated with differences in the ground temperatures as well as differences in the low-level stability characteristics.

6. ACKNOWLEDGEMENT

This research was partially supported by the USDA Forest Service, through a cooperative agreement with the Southern Research Station. We thank Wilfredo Blanco of the FSU Visualization Laboratory for assistance in creating Figs. 2–6.

7. REFERENCES

Clark, T. L., Jenkins, M. A., Coen, J., and Packham, D, 1996: A Couple atmosphere-fire model: convective feedback on fire-line dynamics. *Journal of Applied Meteorology*, **35,** 875–901.

Haines, D. S., 1988: A lower atmospheric severity index for wildfires. *National Weather Digest*, **13(2),** 23–27.

Linn, R. R., 1997: A transport model for prediction of wildfire behavior. Ph.D dissertation, New Mexico State University, 195 pp. [Available from Los Alamos National Laboratory, LA-13334-T.]

Linn, R. R., Reisner, J., Colman, J. J., and Winterkamp J., 2002: Studying wildfire behavior using FIRETEC. *International Journal of Wildland fire,* **11**, 233–246.

Jenkins, M. A., 2001: Coupled atmosphere-fire modeling and fire behavior sensitivity to atmospheric instability. Preprints, *4th Symposium on Fire and Forest Meteorology*, Reno, NV.

Potter, B. E., 1996: Atmospheric properties associated with large wildfires. *International Journal of Wildland fire*, **6(2)**, 71-76.

Reisner, J., Wynne, S., Margolin, L., and Linn, R. R., 2000: Coupled atmospheric-fire modeling employing the method of averages. *Monthly Weather Review*, **128**, 3683-3691.

Werth, J., and Ochoa, R., 1993: The evaluation of Idaho wildfire growth using the Haines Index. *Weather and Forecasting,* **8(2)**, 223-234.

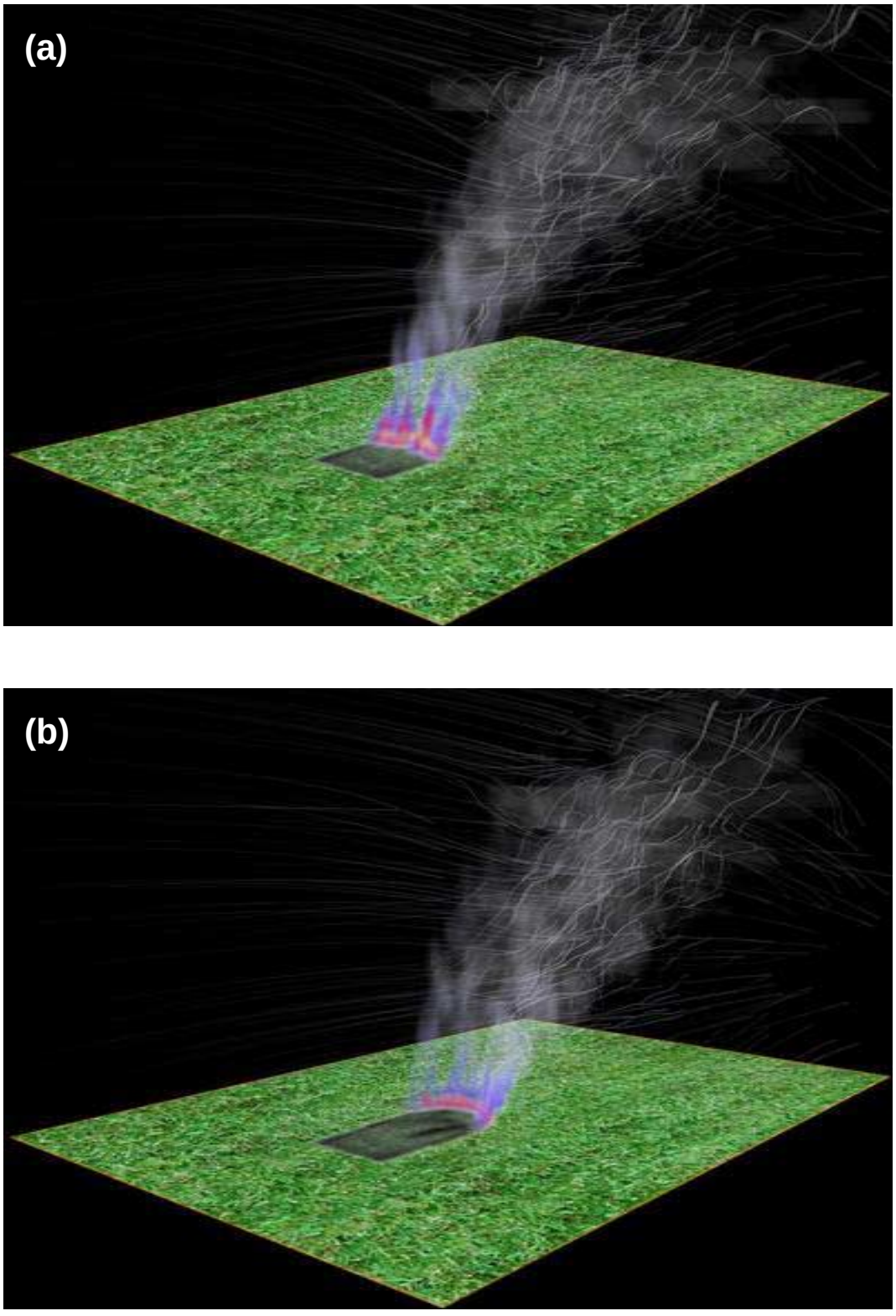

Figure 2. Images for the temperature and streamline in the domain, and the fuel density on the ground for the neutral case, at (a) t = 120 s and (b) t = 240 s. (Image by FSU Visualization Laboratory.)

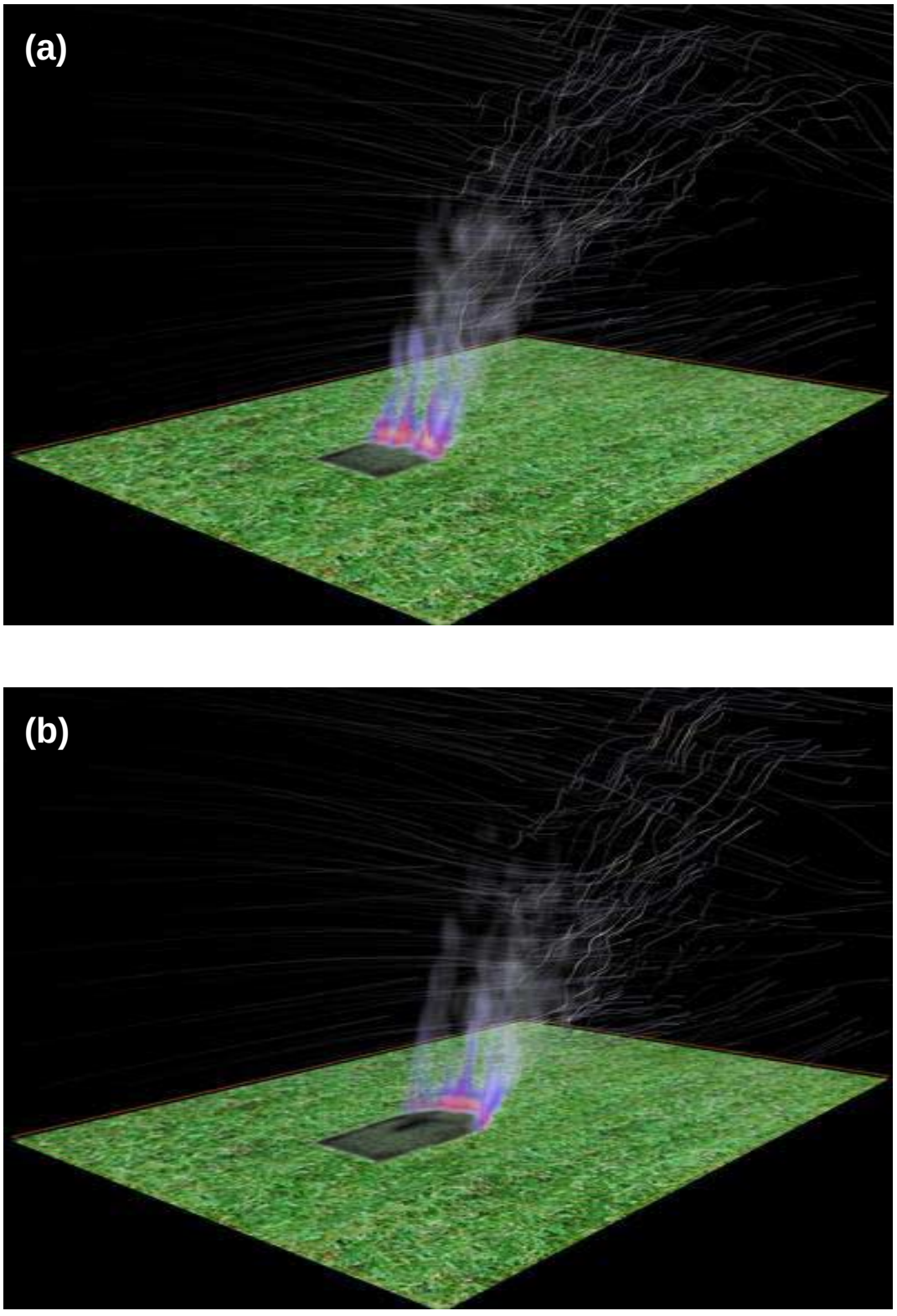

Figure 3. Images for the temperature and streamline in the domain, and the fuel density on the ground for the stable case I, at (a) t = 120 s and (b) t = 240 s. (Image by FSU Visualization Laboratory.)

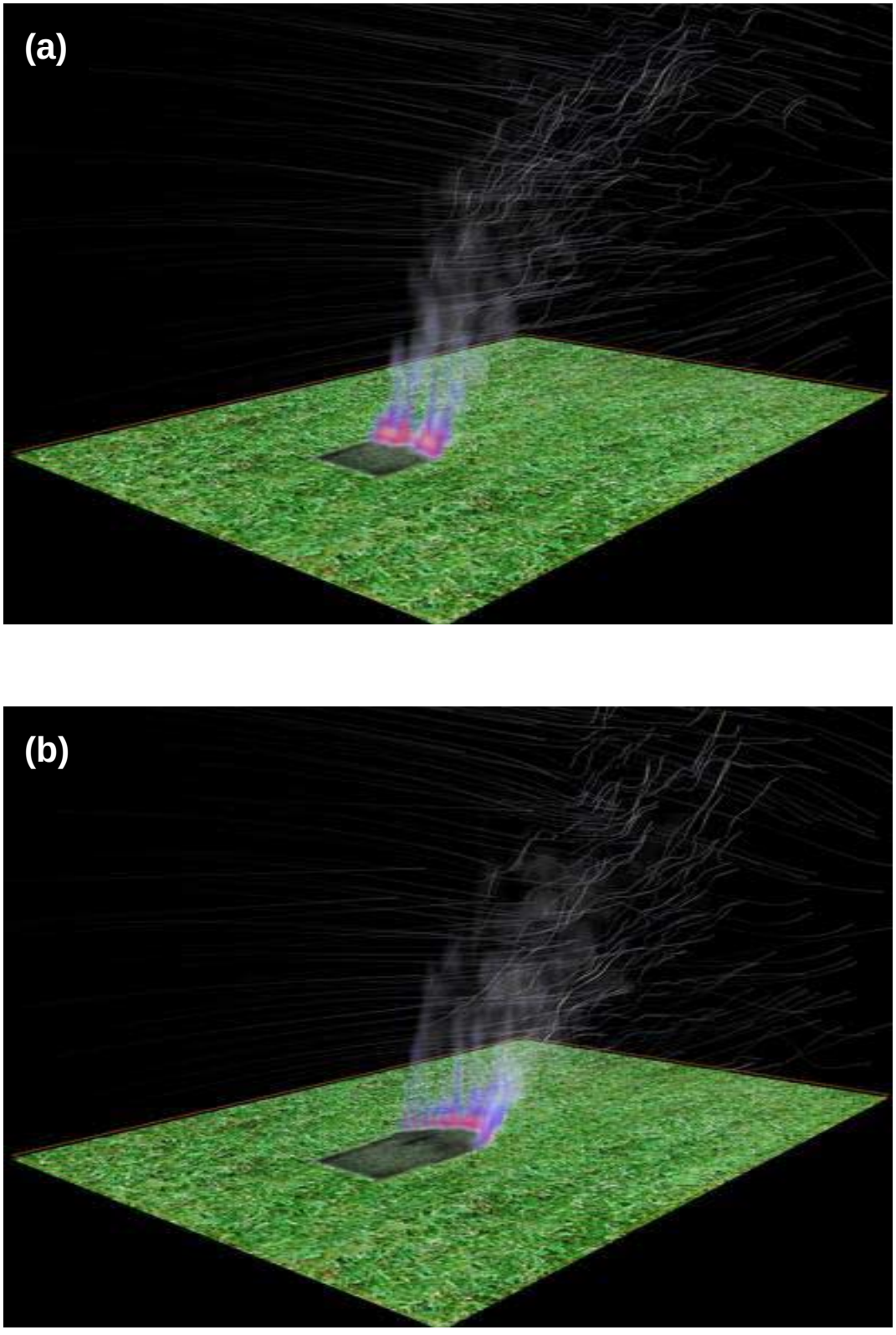

Figure 4. Images for the temperature and streamline in the domain, and the fuel density on the ground for the stable case II, at (a) t = 120 s and (b) t = 240 s. (Image by FSU Visualization Laboratory.)

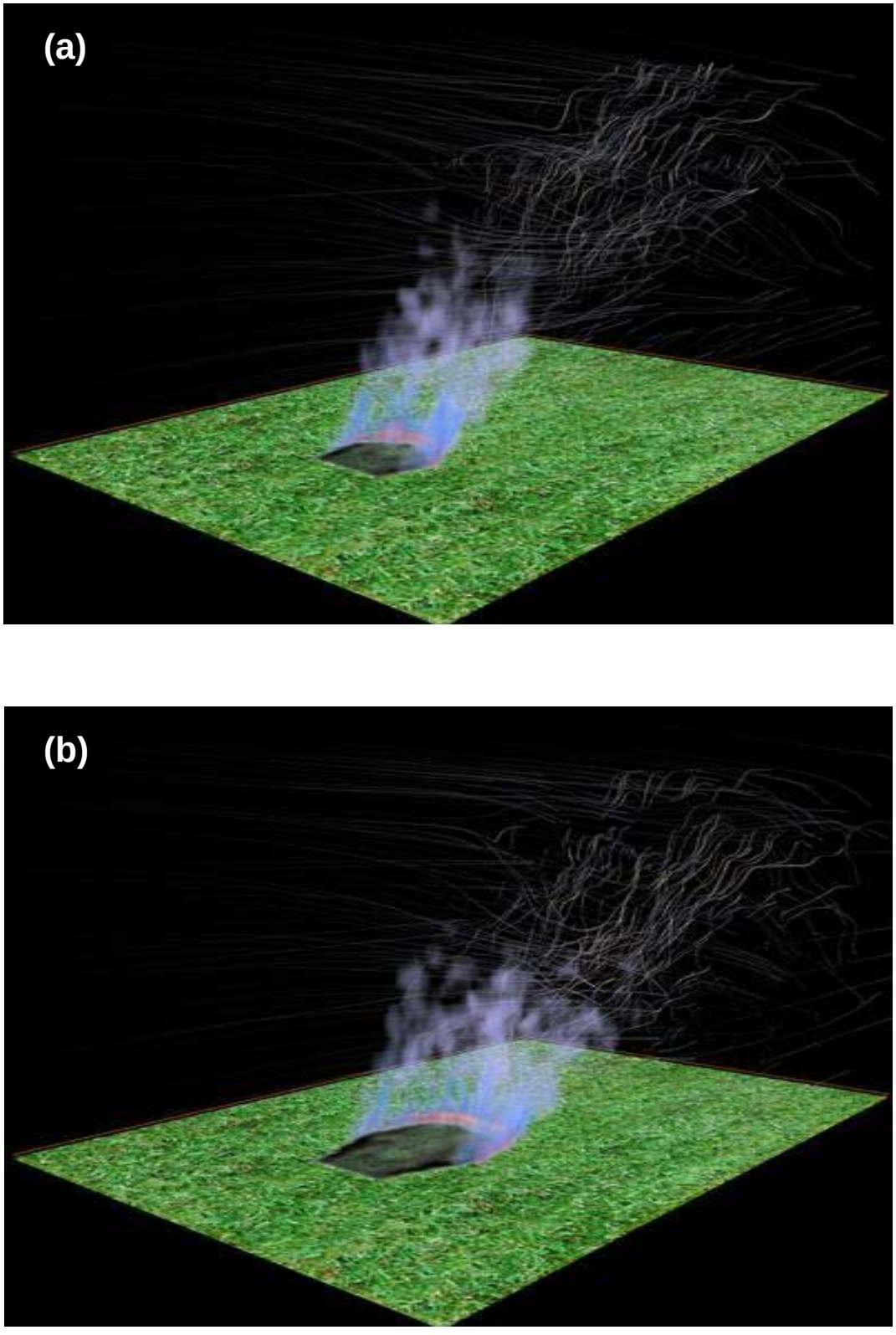

Figure 5. Images for the temperature and streamline in the domain, and the fuel density on the ground for the unstable case I, at (a) t = 120 s and (b) t = 240 s. (Image by FSU Visualization Laboratory.)

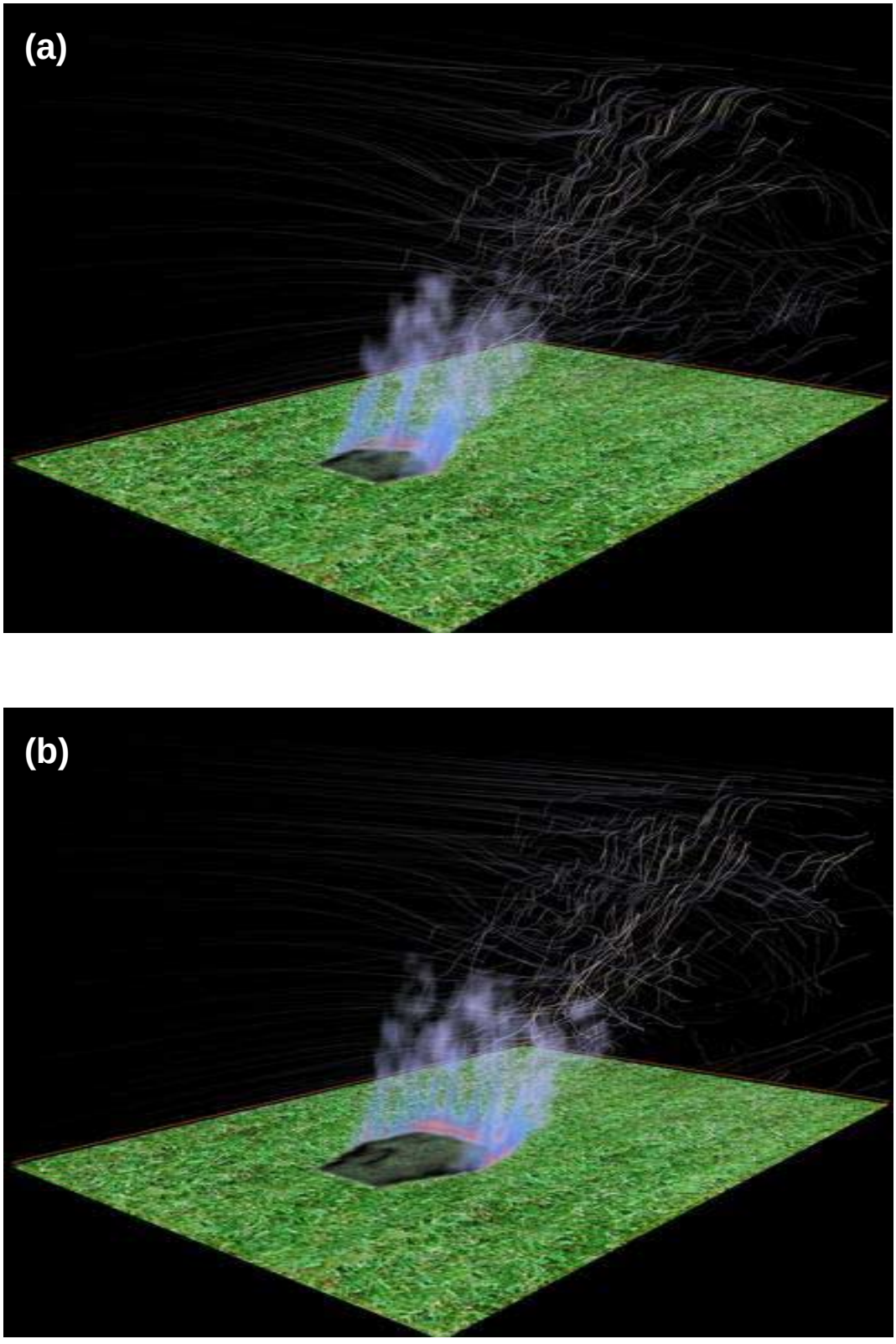

Figure 6. Images for the temperature and streamline in the domain, and the fuel density on the ground for the unstable case II, at (a) t = 120 s and (b) t = 240 s. (Image by FSU Visualization Laboratory.)

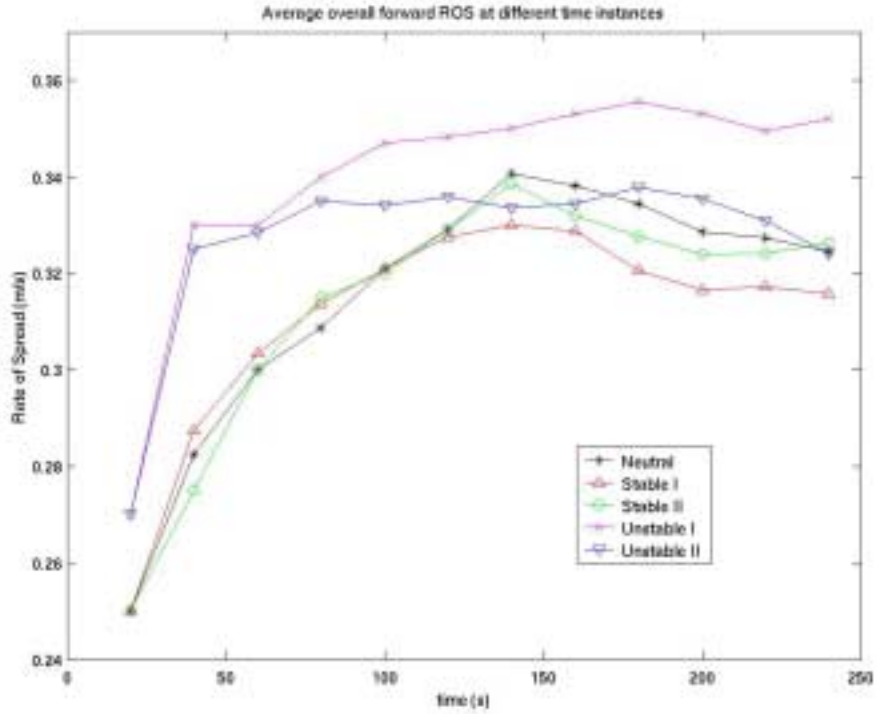

Figure 7. Variation of the average overall ROS in the wind direction over the 20 ignition cells with time for different cases.

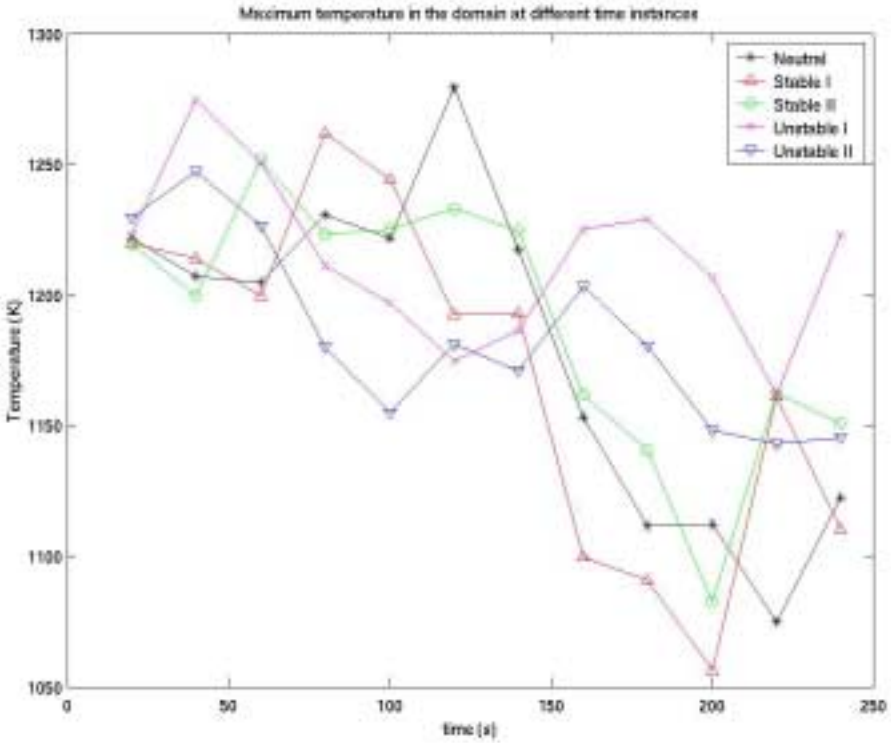

Figure 8. Variation of maximum potential temperature in the domain with time for different cases